Filter Designs for a Reconfigurable Photonic Integrated Circuit

Yujia Wang, John J. Shynk, Larry A. Coldren
Department of Electrical and Computer Engineering
University of California
Santa Barbara, CA 93106-9560

***Abstract*— This paper presents non-classical bandpass filter designs for a reconfigurable photonic integrated circuit (PIC). Because the designs must be realizable for a high frequency range in a new optical device, we consider digital infinite-impulse response filters that avoid lasing for a specific unit cell configuration. In order to accommodate the architecture of the PIC, we describe a design procedure for bandpass filters in the 10 GHz frequency range based on a prototype filter constructed from second-order sections.**

I. Introduction

For future signal processing platforms, it will be necessary to design filter structures that operate at frequencies near 10 GHz and with bandwidths around 50 MHz. Although optical infinite-impulse-response (IIR) and finite-impulse-response (FIR) filter architectures have previously been proposed [1]–[4], no photonic integrated circuits (PICs) have been physically realized. However, with recent advances in PIC technology, it is anticipated that filters in this frequency range can be implemented using a cascade of unit cells. In order to model such devices, we consider bandpass filter designs that fulfill these requirements while maintaining normal operation without lasing.

For a reconfigurable PIC, device elements that provide independent control of the magnitude and phase of the poles and zeros of an IIR system are needed. To achieve this, the unit cell is integrated with the following elements as shown in Figure 1: multi-mode interference (MMI) coupler [5], semiconductor optical amplifier (SOA) [6], and phase modulator (PM) [7]. The component operations can be described as functions of the input signal wavelength, yielding optical-response characteristics. To match the response of the physical device to that of a digital filter design, we employ a z-transform model to derive the correct mapping of the PIC parameters. The mapping is based on the bilinear transform, which connects the digital and analog domains via the sampling frequency f_s, which in turn is related to the free spectral range (FSR) of the optical system [8], [9]. For the particular unit cell considered here, we assume that $f_s = 25$ GHz.

A PIC operating in the frequency range of 10 GHz is vulnerable to lasing, which is the condition where the device operates as a laser rather than yielding an optical signal that can be processed [10]. Methods of mapping between the optical and signal processing domains were explored in [8], [9], but the need to avoiding lasing for our particular device has not been examined. We have developed mapping strategies for the unit cell, which are independent of the results in [8], [9]. At the desired operating frequency range and with a sufficiently large sampling frequency, classical IIR filter designs result in poles that are very close to the unit circle. These poles in turn correspond to component parameters of the PIC that can cause lasing. To address this issue, we modify the poles and zeros that result from classical designs, such as the elliptic filter, to obtain a magnitude response that has a suitable passband, while avoiding lasing.

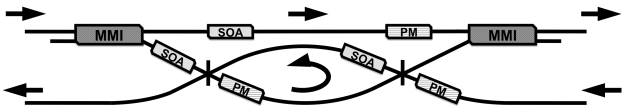

Fig. 1. Unit cell configuration and its signal flow.

The rest of this paper is organized as follows. Section II explains the basic operation and structure of a PIC unit cell, and briefly describes its components. This section also provides an overview of the basic Fabry-Perot etalon [11]. Section III presents filter design techniques and a parameter mapping for governing the behavior of the physical unit cell. The Fabry-Perot etalon is used to demonstrate the relationship between an optical scattering coefficient and the z-domain transfer function. Example results of the designs and responses of the PIC are shown in Section IV, and Section V provides a summary of the filter design.

II. Photonic Filter Overview

A PIC processes information signals carried on optical wavelengths in the visible spectrum. The structure under consideration here consists of a cascade of unit cells, each of which can be viewed as the basic building block of the overall system. A unit cell functions similar to a second-order IIR system providing individually controllable poles and zeros, and has the three previously-mentioned components: MMI, SOA, and PM. The MMI is an optical device that splits or combines its input signals [5], and is characterized by a transmission coefficient and a coupling coefficient. The SOA provides a signal gain, whereas the PM changes the phase [6], [7]. The arrangement of the MMI, SOA, and PM for the unit cell considered here is shown in Figure 1. With these

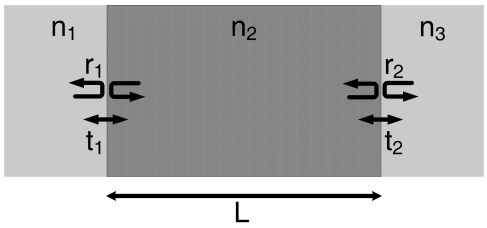

Fig. 2. Fabry-Perot etalon and its signal flow.

three components, feedforward and feedback structures can be implemented and reconfigured to process optical signals.

The input-output relationship of an optical system is modeled by a scattering coefficient [11]. To demonstrate the use of a scattering coefficient for signal processing, we examine a basic optical element known as the Fabry-Perot etalon, which functions as a simple optical narrowband filter. It is characterized by two sets of reflection and transmission coefficients $\{t_1, r_1, t_2, r_2\}$, the length L of the device, and the propagation constant $\tilde{\beta}$ of the material [11]. Figure 2 shows a block diagram of the Fabry-Perot etalon and its signal flow.

The etalon is typically made of two reflecting surfaces. When an incident signal $s(t)$ strikes the interface of the etalon from either material with index n_1 or n_3, part of the signal will reflect according to $rs(t)$, while the rest transmits through as $ts(t)$, where r and t satisfy $r^2 + t^2 = 1$. Inside the etalon, the signal magnitude and phase will change due to properties of the material according to $e^{-j\tilde{\beta}L}$, where $\tilde{\beta}$ is the complex propagation constant of the material with index n_2. Example indices are $n_1 = n_3 = 1.0003$ for air and $n_2 = 4.24$ for silicon. For a symmetric ($r_1 = r_2$) and lossless ($\beta_i = 0$) Fabry-Perot etalon, Figure 3 shows the optical response of the structure conveyed by the transmission coefficient S_{21} described in the next section. Observe that it is a periodic function of βL where β is the attenuation component of $\tilde{\beta}$.

The spacing between two adjacent resonator modes, known as the free spectral range (FSR) [11], is given by $\mathrm{FSR} = c/2nL$ where c is the speed of light, n is the index of the material, and L is the length of the device. As seen in Figure 3, the FSR corresponds to one period of the plot; the repeating nature of the optical pole graph translates to an inherent sampling frequency of $f_s = \mathrm{FSR}$. With knowledge of the parameters of the device and its optical behavior, we can establish a correspondence between the optical response and a z-domain transfer function and thus the corresponding frequency response.

The problem of lasing must be considered when designing digital filters for the unit cell. Because feedback is needed to create an IIR filter response, the unit cell contains a loop configuration in the design. Since a loop results in an internal power loss for the optical signal, an SOA is integrated into the design. Lasing refers to the condition when the gain and loss within the loop are equal, resulting in an output that is independent of the input. The effect of lasing is closely related to the instability of a digital filter with feedback. Therefore, one must design the IIR filter poles to be sufficiently within the

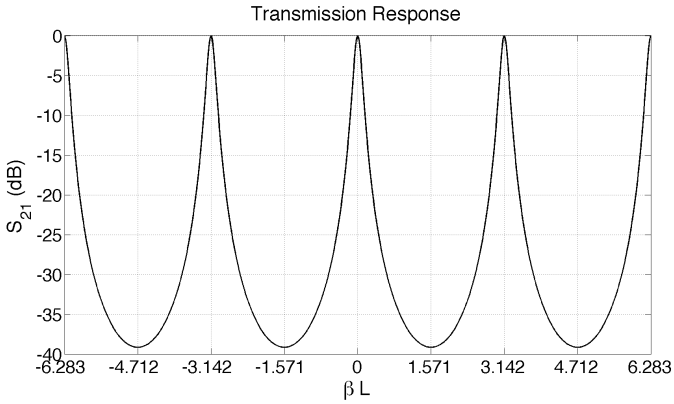

Fig. 3. Fabry-Perot transmission response showing pole locations.

unit circle in the z-plane. For our unit cell, we have determined that the pole magnitudes should be constrained to be < 0.995 in order to provide a margin of safety.

III. Photonic Integrated Circuit

A. Basic Filter Design

The bandpass filter design requirements of interest are the following: 10 GHz center frequency, 50 MHz resolution, and 60 dB stopband attenuation. Using a twelfth-order elliptic filter and a 40 ps sampling period, we are able to meet the design criteria. However, the resulting classical filter structure has pole magnitudes exceeding 0.995, which may cause the PIC to exceed the lasing threshold. As a result, we use the elliptic filter for a prototype design and derive a suboptimal filter by adjusting the pole magnitudes.

B. Cascade System

The design is based on a cascade of second-order elliptic filter sections. The transfer function of a second-order all-pole system can be written in the s-domain as

$$H(s) = \frac{1}{s^2 + 2\zeta\omega_o s + \omega_o^2}, \tag{1}$$

which is characterized by the cutoff frequency ω_o (natural frequency) and the sharpness of the peak ζ (damping ratio). Since the poles occur as a complex conjugate pair of the form $-\sigma \pm j\omega$, (1) can be written as

$$H(s) = \frac{1}{s^2 + 2\sigma s + (\sigma^2 + \omega^2)} \tag{2}$$

where

$$\sigma = \zeta\omega_o \tag{3}$$

$$\omega = \omega_o\sqrt{1-\zeta^2}. \tag{4}$$

A cascade of second-order sections translates to fabricated unit cells with a more rapid and stable configuration than that possible using coupled resonators. The architecture of the unit cell is based on using a second-order section as the basic component of the filter design.

C. Pole Constraint

In the digital filter design, we must take into consideration that the pole magnitudes should not exceed 0.995 in the z-domain in order to avoid lasing. To determine the corresponding constraint on the pole locations, we start with the bilinear transform that connects a digital design to the poles in the s-domain, i.e.,

$$\begin{aligned} z &= \frac{1+\frac{T_s}{2}s}{1-\frac{T_s}{2}s} \\ &= \frac{1-\sigma\frac{T_s}{2}+j\omega\frac{T_s}{2}}{1+\sigma\frac{T_s}{2}-j\omega\frac{T_s}{2}} \end{aligned} \tag{5}$$

where T_s is the sampling period. Since the magnitude of z is < 0.995, this corresponds to

$$\frac{\sqrt{\left(1-\sigma\frac{T_s}{2}\right)^2+\left(\omega\frac{T_s}{2}\right)^2}}{\sqrt{\left(1+\sigma\frac{T_s}{2}\right)^2+\left(\omega\frac{T_s}{2}\right)^2}} < 0.995. \tag{6}$$

After a few equation manipulations, we arrive at the following expression:

$$\left(\sigma-\frac{398}{T_s}\right)^2+\omega^2 < \frac{397.995^2}{T_s^2}, \tag{7}$$

which we see is the equation of a circle. As shown in Figure 4, the region of the constrained poles is entirely to the left of the imaginary axis, which is required for general stability, and is vertically centered about the real axis to allow for a complex conjugate pair. Observe that the poles are constrained to be further away from the imaginary axis with increasing frequency.

D. Parameter Mapping

We can establish a connection between the optical characteristics of the unit cell and its z-domain response by examining the Fabry-Perot etalon. The signal flow of this device is modeled using scattering coefficients [11], which provide the relationships between signals at the input and output ports. Although the etalon has two input ports and two output ports (such that a signal can enter or exit the device from material n_1 or n_3), initially we are interested in the relationship between input port 1 and output port 2, as indicated in Figure 2. The other input and output ports typically involve feedback signals in a cascade structure, and thus they are not of interest for a standalone etalon. The scattering coefficient from port 1 to port 2 is

$$S_{21} = \frac{t_1 t_2 e^{-j\tilde{\beta}L}}{1-r_1 r_2 e^{-2j\tilde{\beta}L}} \tag{8}$$

where $\{t_1, t_2\}$ are the transmission coefficients, $\{r_1, r_2\}$ are the reflection coefficients, and

$$\tilde{\beta} = \beta + j\beta_i \tag{9}$$

is the propagation constant of the material characterized by the attenuation constant β and the phase constant β_i. The real part of $e^{-2j\tilde{\beta}L}$ can be factored out such that

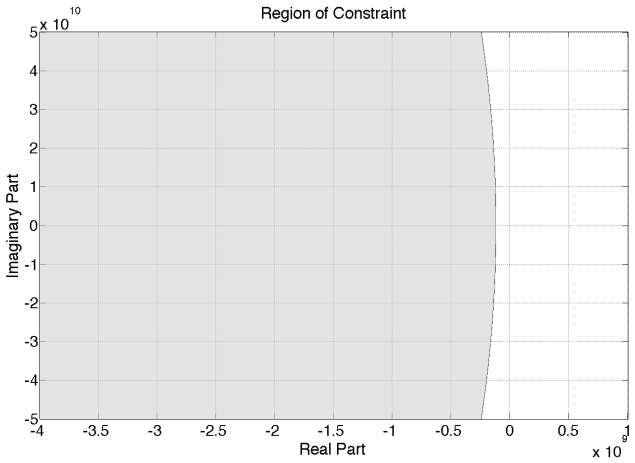

Fig. 4. Constrained pole region in the s-plane due to (7) with $T_s = 40$ ps.

$$S_{21} = \frac{t_1 t_2 e^{\beta_i L} e^{-j\beta L}}{1-r_1 r_2 e^{2\beta_i L} e^{-2j\beta L}}, \tag{10}$$

and since $t_1^2 + r_1^2 = t_2^2 + r_2^2 = 1$, we can write

$$S_{21} = \frac{\sqrt{1-r_1^2}\sqrt{1-r_2^2} e^{\beta_i L} e^{-j\beta L}}{1-r_1 r_2 e^{2\beta_i L} e^{-2j\beta L}}. \tag{11}$$

The scattering coefficient S_{21} describes the relationship between the input signal and the output signal as a function of wavelength. When designing a digital filter, we are interested in the z-domain response. To obtain the proper conversion, note that the smallest unit of time is the delay of a signal through the etalon of length L. Thus, βL is the fundamental frequency of the system, so that in z-domain we have the transfer function

$$H_{21}(z) = \frac{\sqrt{1-r_1^2}\sqrt{1-r_2^2} e^{\beta_i L} z^{-T}}{1-r_1 r_2 e^{2\beta_i L} z^{-2T}} \tag{12}$$

where z^{-T} corresponds to the fundamental delay of the system. For this particular structure, there is a single zero $z_1 = 0$ and two poles $p_{1,2} = \pm\sqrt{r_1 r_2} e^{\beta_i L}$. The Fabry-Perot etalon is a simple structure that demonstrates how to map from a scattering coefficient to the transfer function in the z-domain. The process can be extended to the more complicated unit cell used in the PIC and derived from a combination of MMIs, SOAs, and PMs. These elements allow for control of the pole and zero locations in the PIC, and thus we can design digital filters that model and govern the behavior of the optical system.

IV. Example Results

The following filter design results were obtained by first constructing an elliptic filter with six cascaded second-order sections, and then adjusting the pole magnitudes. The angular locations of the poles were kept the same while the ζ value for each section was modified to meet the magnitude constraint to avoid lasing. The zeros were then moved to different frequencies so that their effect on the rise of the passband

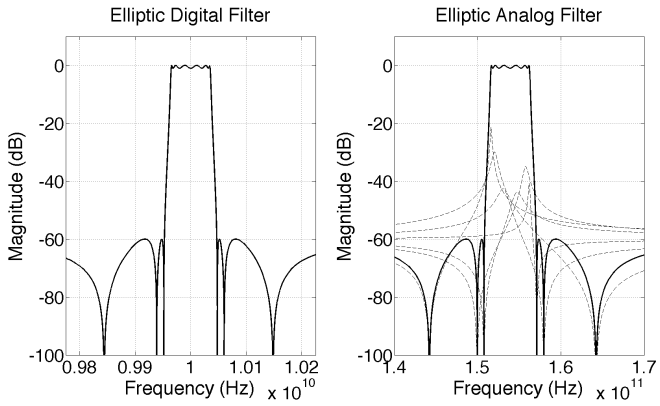

Fig. 5. Digital and analog elliptic filter designs. The dotted lines indicate the responses for the second-order sections.

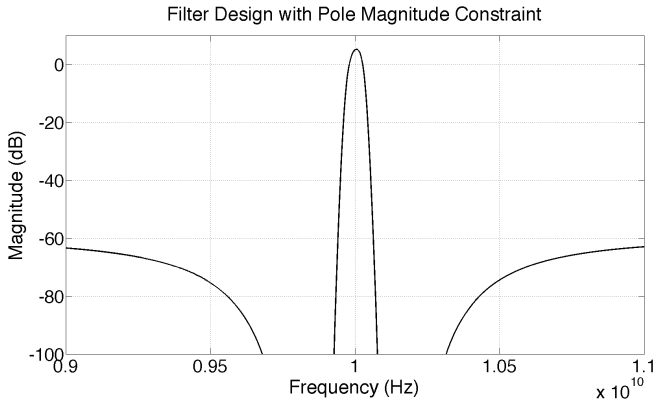

Fig. 6. Frequency response of the filter design with a pole magnitude constraint.

was minimized. Figure 5 shows the original digital and analog designs; the resulting filter response that meets the 0.995 magnitude constraint is provided in Figure 6. Figure 7 shows the transmission response of the unit cell (similar to that in Figure 3), and Figure 8 is the corresponding digital filter frequency response.

V. Conclusion

We considered design methods for a reconfigurable optical filter consisting of unit cells that contain SOAs, MMIs, and PMs. As demonstrated with the Fabry-Perot etalon, the signal flow characteristic of a PIC can be mapped to a transfer function in the z-domain by examining a scattering coefficient. In order to model and govern the PIC's operation, we considered a twelfth-order elliptic bandpass filter with a 10 GHz center frequency, a 50 MHz resolution, and a 60 dB stopband attenuation. However, due to the possibility of lasing in the device, we derived a suboptimal filter from this prototype design that constrains the pole magnitudes to be < 0.995. This design that can be physically realized in an optical filter operating in the 10 GHz range without causing lasing.

VI. Acknowledgments

The authors would like to thank J. Bovington, H.-W. Chen, A. Fang, and R. Guzzon for helpful discussions. This work was supported by the Defense Advanced Research Projects Agency under Grant HR0011-08-1-0006.

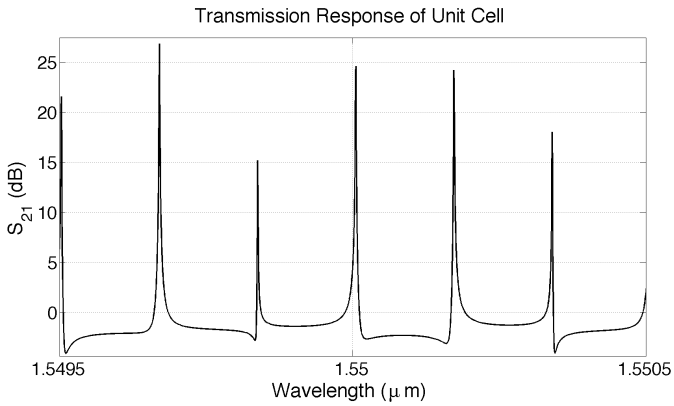

Fig. 7. Unit cell transmission response showing the pole locations.

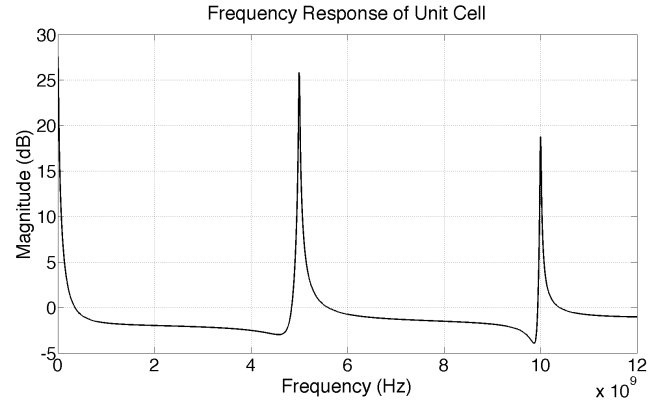

Fig. 8. Unit cell frequency response showing the pole locations.

References

[1] J. E. Bowers, S. A. Newton, W. V. Sorin, and H. J. Shaw, "Filter response of single-mode fibre recirculating delay lines," *Electronics Letters*, vol. 18, pp. 110–111, Feb. 1982.

[2] M. Tur, J. W. Goodman, B. Moslehi, J. E. Bowers, and H. J. Shaw, "Fiber-optic signal processor with applications to matrix-vector multiplication and lattice filtering," *Optics Letters*, vol. 7, pp. 463–465, Sept. 1982.

[3] Y. Fainman and S. H. Lee, "Experimental evaluation of Mangin mirror performances for optical processing with feedback," *Optical Engineering*, vol. 24, pp. 535–540, 1985.

[4] H. Rajbenbach, Y. Fainman, and S. H. Lee, "Optical implementation of an iterative algorithm for matrix inversion," *Applied Optics*, vol. 26, pp. 1024–1031, 1987.

[5] L. B. Soldano and E. C. M. Pennings, "Optical multi-mode interference devices based on self-imaging: Principles and applications," *Journal of Lightwave Technology*, vol. 13, no. 4, pp. 615–627, Apr. 1995.

[6] M. J. Connely, *Semiconductor Optical Amplifiers*. New York: Springer, 2002.

[7] K.-P. Ho, *Phase-Modulated Optical Communication Systems*. New York: Springer, 2005.

[8] C. K. Madsen and J. H. Zhao, *Optical Filter Design and Analysis: A Signal Processing Approach*. New York: Wiley, 1999.

[9] G. Pasrija, Y. Chen, B. Farhang-Boroujeny, and S. Blair, "DSP approach to the design of nonlinear optical devices," *EURASIP Journal on Applied Signal Processing*, vol. 10, pp. 1485–1497, 2005.

[10] W. Koechner, *Solid-State Laser Engineering*. New York: Springer, 2006.

[11] L. A. Coldren and S. W. Corzine, *Diode Lasers and Photonic Integrated Circuits*. New York: Wiley, 1995.